# Nonexponential dephasing in a local random matrix model

Vance Wong[1] and Martin Gruebele[2]
[1]*Department of Chemistry and Beckman Institute for Advanced Science and Technology, Urbana, Illinois 61801*
[2]*Department of Chemistry, Physics, Biophysics, and Beckman Institute for Advanced Science and Technology, Urbana, Illinois 61801*
(Received 29 June 2000; published 4 January 2001)

Deviations from exponential decay dynamics have been proposed for a wide variety of systems in high-energy, atomic, and molecular physics. This work examines the quantum dynamics of a simple hierarchical local random matrix model. The hierarchical structure is imposed by two physically motivated constraints: an exponential size scaling of matrix elements, and a quantum number ''triangle rule,'' which introduces correlations in the quantum-state space by mimicking the nodal structure of wave functions in a coordinate Hamiltonian. These correlations lead to a systematic slowing of dephasing dynamics compared to exponential decays. A generalized Lorentzian line shape is introduced as the Fourier transform of a polynomial survival amplitude to describe the average behavior of these decays. The model is brought into a representation that can be compared directly with the golden rule. In this representation, the deviations from exponentiality arise from energy-dependent correlations among the coupling matrix elements that persist even for large systems. Finally, the effects of relaxing the size scaling and ''triangle rule'' constraints are studied. Sparsity of the random matrix alone is not sufficient to produce slow asymptotic dynamics; both types of constraints are required.

DOI: 10.1103/PhysRevA.63.022502 PACS number(s): 33.70.−w, 03.65.−w, 05.60.Gg

## I. INTRODUCTION

The relaxation of a quantum state coupled to a dense manifold is often approximated by an exponential decay of the initially prepared state. Such approximate models include the Redfield equations and the first-order golden rule. Examination of real physical situations shows that in many circumstances, the actual decay $P(t)$ becomes nonexponential before the asymptotic value of $P(t)$ is reached. Examples include certain autoionizing atomic states [1], asymptotic decays in field theories studied by nonperturbative approaches [2], decoherence of spin-boson systems at low temperature [3], or for certain Kondo parameters [4], diffusion of wave packets corresponding to molecular vibrational motions [5,6], and dynamics of kicked rotators [7]. Asymptotically, these phenomena are best described by a power law $P(t) \sim t^{-\delta/2}$ instead of an exponential function. (The factor of 1/2 is included in the exponent if one wishes to make a connection to the classical theory of diffusion processes.)

The existence of nonexponential dephasing has potentially important physical implications. For scalar fields producing bosons, it can lead to dynamical multiparticle condensation [2]. In quantum computing, asymptotically slow increase of incoherence due to a bath could extend the temporal limits of computability. In molecules, slow dephasing of the vibrations allows the possibility of controlling the reactivity through coherent laser excitation [8,9].

The temporal hierarchy of a power law implies a hierarchical structure of the underlying Hamiltonian [10–12], which in turn implies a hierarchical structure of its matrix representation. Although exponential decay can be studied by global random matrices [13], power laws require a hierarchical local random matrix (HLRM) as a minimal model. Such models arise quite naturally in the study of many-dimensional quantum systems. For example, the chemical bonds in molecules are often highly localized and can be approximated by coupled electron pairs. Vibrational energy is therefore locally transferred through the lattice of molecular bonds, connecting the atoms [5]; the nominal connectivity of this lattice is quite low (usually 1–4 bonds per atom in organic molecules).

We investigate the minimal requirements that a HLRM model must satisfy in order to produce asymptotically slow dephasing dynamics of quantum wave packets propagated under the HLRM. As it turns out, a HLRM model introduces energy-dependent correlations among the amplitudes of states of the spectrum that represents the quantum system. The local structure of the matrix ensures that these correlations do not die off as the size of the quantum system is increased, so spectral correlations persist even in multidimensional quantum systems [14].

Section II introduces some preliminaries needed in the analysis of our HLRM model. A generalized Lorentzian line shape is introduced that corresponds to power-law decays in the time domain. It is chosen to yield an exponential decay in the limit $\delta \to \infty$, thereby making it a useful unbiased fitting function for spectral representations of the HLRM. The Lawrance-Knight-Lehmann (LKL) inversion procedure [15,16] is used to see how this line shape affects matrix element distributions in a ''golden rule'' basis. Finally, a simple example of matrix randomization shows how the removal of spectral correlations reduces the stretched dynamics to simple exponentials. Section III discusses our HLRM, the previously defined Bose-statistics-triangle-rule model (BSTR) [17]. This model uses simple rules for the construction of an ensemble of Hamiltonian matrices. The rules were chosen because they are approximately obeyed by a number of real physical systems. The model produces initial exponential deflation of the survival probability of nonstationary states, followed by slow asymptotic dynamics as the wave packet reaches the ''statistical limit.'' A numerical study of BSTR quantum dynamics is presented, together with an ex-

 

amination of the effect of relaxing the model's rules. The model is also examined in a ''golden rule'' basis, allowing us to study the spectral correlations directly, and the consequences of destroying such correlations. Section IV discusses these results, and presents some experimentally studied examples that range from nuclear magnetic resonance spectra of proteins to vibrational spectra of highly excited molecules.

## II. PRELIMINARIES

### A. Spectrum and time evolution

Quantum systems such as molecules, semiconductors, or nuclei are usually studied experimentally via their spectra. To establish a link with experiment, we therefore consider the asymptotic dynamics from the point of view of the spectrum $I(\omega)$, or of the time-dependent decay $P(t)$ of an initially prepared state. Consider a bound quantum system with Hamiltonian $\hat{H}$, spectrum $\{\omega_e\}$, and dipole operator $\hat{\mu}$. Let the system initially be in a state $|g\rangle$. Interaction with a weak frequency-tunable field allows population of excited eigenstates $|e\rangle$ of $\hat{H}$ with intensity proportional to

$$I(\omega)=\sum_e |\langle e|\hat{\mu}|g\rangle|^2 \delta(\omega-\omega_e). \tag{1}$$

The summation notation assumes a finite density of states (although in practice a potentially very large one). Equation (1) neglects radiative decay or other couplings external to the system (hence the $\delta$ function in the summation). Nevertheless, processes describable as relaxation or dephasing can occur within the system as follows. The magnitude of the coupling amplitudes $\langle e|\hat{\mu}|g\rangle$ may be peaked in a spectral region $\Delta\omega$ covering a large number of eigenstates $|e\rangle$: the spectrum in this region contains a line shape. Associated with that line shape is a state $|0\rangle$ located at $\omega_0$. $|0\rangle$ is obtained by defining a distorted initial state $|\phi\rangle=\hat{\mu}|g\rangle$, and a projection operator $\mathcal{P}=\Sigma'|e\rangle\langle e|$ summing over the interval $\Delta\omega$, such that $|0\rangle=\mathcal{P}|\phi\rangle$ [18]. $|0\rangle$ is the state that carries the oscillator strength in the region $\Delta\omega$, and it is nonstationary. Its survival probability is given by

$$P(t)=|\langle 0|e^{-iHt/\hbar}|0\rangle|^2=|\langle 0|t\rangle|^2. \tag{2}$$

Experimentally, one could excite this state with a short, chirp-free optical pulse centered at $\omega_0$ and of bandwidth greater than $\Delta\omega$. $P(t)$ decreases as this initial state dephases according to Eq. (2). Alternatively, one could speak of relaxation of population out of $|0\rangle$ into an orthogonal manifold $\{|s\rangle\}$ in the interval $\Delta\omega$. The line shape $I(\omega)$ is related to the survival amplitude $\langle 0|t\rangle$ by Fourier transform.

The state $|0\rangle$ and its orthogonal ''dark'' manifold $\{|s\rangle\}$ are easily constructed from the $N$ eigenvalues $\omega_e$ and intensities $I_e=|\langle e|\hat{\mu}|g\rangle|^2$ in the interval $\Delta\omega$ via the LKL inversion. In the resulting ''golden rule'' representation, the initial state $|0\rangle$ is coupled by $N-1$ coupling constants $V_{0s}$ to a prediagonalized manifold of $N-1$ states $|s\rangle$ at $\omega_s$. If the $\omega_s$ and $V_{0s}$ are sufficiently randomly distributed, the well-known result from first-order time-dependent perturbation theory is the golden rule

$$P(t)=(1-\sigma)e^{-kt}+\sigma, \tag{3a}$$

$$k=2\pi\rho\langle V_{0s}\rangle_{\mathrm{rms}}^2/\hbar. \tag{3b}$$

The constant $\sigma$ arises if the density of states $\rho$ is finite because $P(t)$ cannot decay to an average value lower than the number of states $|e\rangle$ under the spectral envelope; $\langle\ \rangle_{\mathrm{rms}}$ indicates a root-mean-square average.

The line shape that corresponds to Eq. (3a) (with the long-time average removed) is a Lorentzian

$$L_\infty=\frac{\pi^{-1}k/2}{(k/2)^2+\omega^2}, \tag{4}$$

centered in the interval $\Delta\omega$ at $\omega_0=0$ for convenience. One possible deviation from this line shape results from spectral truncation, i.e., if the interval $\Delta\omega$ is not sufficiently much larger than $k$. Indeed, such truncation effects are a major source for the deviation of certain atomic autoionization spectra from Eq. (4) [1]. In this paper we are not concerned with truncation effects, but correlations between $\omega_s$ and $V_{0s}$ instead.

### B. Generalized Lorentzian

Instead of Eq. (3a), consider an asymptotic power-law decay

$$P(t)=(1-\sigma)\left(1+\frac{2kt}{\delta}\right)^{-\delta/2}+\sigma. \tag{5}$$

This approaches Eq. (3a) in the limit $\delta\to\infty$. The corresponding line shape will be termed a generalized Lorentzian $L_{\delta/2}$ and is given by (after eliminating the long-time average)

$$L_{\delta/2}=\frac{1}{\pi}\int_0^{+\infty} dt\cos(\omega t)(1+2kt/\delta)^{-\delta/4}. \tag{6}$$

One can immediately see that the generalized Lorentzian must go to Eq. (4) in the limit of an infinite exponent. Equation (6) is easily expressed in terms of trigonometric integrals and powers of $\omega$. For example,

$$L_4(x=2\omega/k)=\sin(x)/k-2Si(x)\sin(x)/\pi k -2Ci(x)\cos(x)/\pi k. \tag{7}$$

Figure 1 (top) shows a Lorentzian and a generalized Lorentzian for the case $\delta=8$. As expected from the slower long-time dynamics, $L_4$ is more sharply peaked toward the center of the spectrum than the Lorentzian, and smaller at intermediate energy gaps. Asymptotically, all functions $L_{\delta/2}$ have a leading term proportional to $\omega^{-2}$, and hence a long spectral tail. The slow decay dynamics of Eq. (5) are therefore not associated with a narrowing of the spectrum at large energy gaps (bottom). The logarithmic derivatives of all $L_{\delta/2}$ approach zero at the line center, although the line shape can

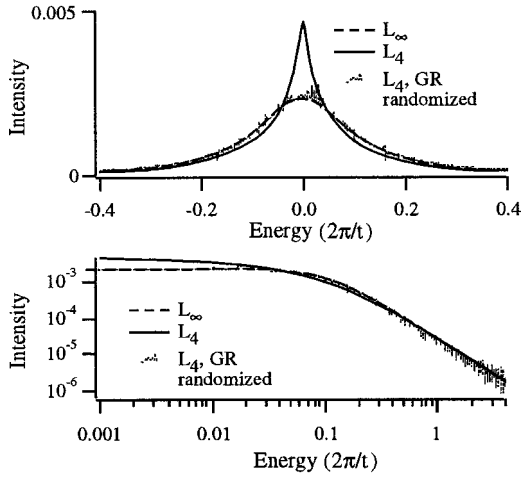


FIG. 1. Intensity vs frequency (in units of $2\pi/t$) plots for $L_\infty$ and $L_4$ line shapes. Randomizing the matrix elements $V_{0s}$ corresponding to $L_4$ as shown in Fig. 3 yields a line shape best fitted by $L_\infty$. Upper plot, linear scale; lower plot, log scale.

have a pronounced cusp for small values of $\delta$. The time domain decays corresponding to Fig. 1 are shown in Fig. 2.

What type of Hamiltonian in the energy range $\Delta\omega$ gives rise to slowed dynamics? This can be answered by applying the LKL inversion to the spectra in Fig. 1, converting them to the prediagonalized golden rule representation. Figure 3 shows that the Lorentzian results in the expected picket fence form of $V_{0s}$, without a dependence of the off-diagonal elements $V_{0s}$ on the energy gap from the initial state. By contrast, the generalized Lorentzian yields a Hamiltonian in which the coupling strength is depleted toward the center. The dependence of $V_{0s}$ on the energy gap is approximately given by a stretched exponential, whose width $W$ and amplitude are inversely related to $\delta$. $W$ and the rms coupling strength $V_{\rm rms}=\{\Sigma_s|V_{0s}^2|\}^{1/2}$ must be of comparable magnitude in order to yield power-law dynamics. In the limit $W\rightarrow 0$, as well as in the limit $W\gg k$, simple exponential dynamics are recovered. The correlation length (on the energy axis) of coupling constants must therefore be comparable to the linewidth, or no deviations from exponential decay can occur.

The asymptotic power-law behavior can therefore be destroyed if the energy-dependent correlation among $V_{0s}$ is removed by shuffling matrix element positions in the Hamiltonian on a scale comparable to the linewidth. This will be

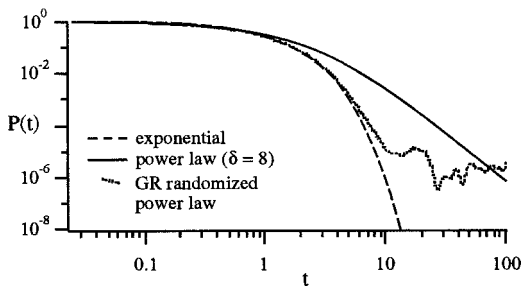


FIG. 2. Survival probabilities $P(t)$ corresponding to the line shapes in Fig. 1.

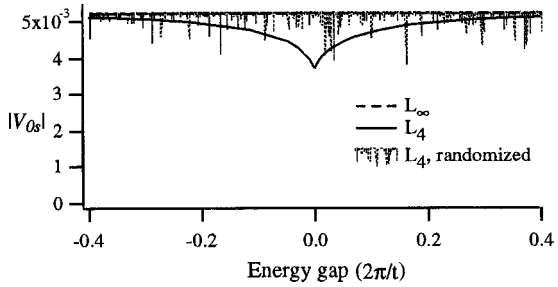


FIG. 3. Absolute value of matrix elements $V_{0s}$ in the ''golden rule'' representation corresponding to the line shapes in Fig. 1.

used in Sec. III to illustrate which part of the slow dynamics is due to the intrinsic structure of the random matrix Hamiltonian, rather than to noise in $P(t)$ resulting from the random choice of matrix elements. It is also illustrated for the simple example discussed here in Figs. 1–3. Figure 3 shows a random distribution of $V_{0s}$ obtained by shuffling the $L_4$ matrix elements shown in the same figure, redistributing the smaller $V_{0s}$ from a window $W$ to the overall window $\Delta\omega$. Figure 1 shows that the spectrum obtained by diagonalization now matches the Lorentzian line shape. Figure 2 shows that the resulting $P(t)$ approaches an exponential decay with a larger baseline $\sigma$. (The calculations were carried out with a finite number of spectral points; the larger value of $\sigma$ observed for the shuffled matrix elements is actually the statistically expected one at the density of states $\rho$ we used; the $\sigma$ is small in the two smooth decays because the evenly spaced frequencies $\omega_s$ lead to a coherent addition of the cosine basis functions of the decay.)

The sensitivity of the long-time dynamics to the assumption of uncorrelated couplings is apparent from the above examples. It remains to be seen under what circumstances an ''uncooked'' model Hamiltonian yields slowed dephasing. We therefore depart from the rather idealized golden rule representation, and investigate a physically motivated HLRM model of dephasing next.

## III. DEPHASING IN A LOCAL RANDOM MATRIX MODEL

### A. The BSTR model

The Bose statistics triangle rule model is a local random matrix model similar to one originally devised to study the dephasing of highly excited molecular vibrational states [17]. The constraints imposed by it on the Hamiltonian are quite generic, and are approximately satisfied in many real systems. The model is defined as follows in terms of its matrix elements $h_{ij}$:

(i) The $h_{ii}$ are Poisson-distributed with average energy spacing $\Delta E$.

(ii) $h_{ij}=\pm Va^{n_{ij}}$ (random signs).

(iii) $n_{ij}$ is normal-distributed with mean $\overline{n}=E/\overline{\omega}$ and variance $\sigma_n^2=2E/\mathcal{N}\overline{\omega}^2$.

(iv) For any triplet $i,j,k$, $|n_{ij}-n_{jk}|\leq n_{ik}\leq|n_{ij}+n_{jk}|$.

$V$, $a$, $E$, $\Delta E$, $\mathcal{N}$, and $\overline{\omega}$ are model parameters. The physical motivation of the model is as follows. Let a quantum system of $\mathcal{N}$, oscillators have a Hamiltonian of the form

$$H=\sum_{m=1}^{\mathcal{N}}\left\{\frac{1}{2}p_m^2+\frac{\hbar}{4}\omega_m q_m^2\right\}+\frac{\lambda}{3!}\sum_{m,p,r=1}^{\mathcal{N}}v_{mpr}q_m q_p q_r + H_2+\lambda H_3+\lambda^2 H_4+\cdots+\lambda^{n-2}H_n+\cdots. \quad (8)$$

The unitless coordinates are given by ladder operators as $q_m=b_m^\dagger+b_m$. $H_2$ has Poisson-distributed eigenvalues in any interval $\Delta\omega$ at sufficiently high energy $E$, as long as the oscillator frequencies are distributed over a sufficiently wide range [19]. The eigenfunctions of $H_2$ in the range $\Delta\omega$ at $E$ have Bose-Einstein distributed quantum numbers $n_m$ in each degree of freedom $m$. As a consequence of the central limit theorem, this results in a normal distribution of the total quantum number difference $n_{ij}=\Sigma_m|n_{im}-n_{jm}|$ between two states, when $\mathcal{N}$ is sufficiently large [17]. The mean and variance of this distribution depend on the energy $E$, dimensionality of the system $\mathcal{N}$, and harmonically averaged frequencies $\omega_i$ as shown in cases (i) and (ii) [17]. Equation (8) is a good model for many systems, such as lattice phonons, molecular vibrations, coupled excitons, or any discretized boson field theory.

The locality of the BSTR model arises from the two constraints [(ii) and (iv)]. Both of these introduce averaged knowledge about the nodal structure of eigenfunctions of $H_2$ into the BSTR matrix structure. First, because the coupling terms are smooth coordinate functions, coupling matrix elements drop off with order $n$ by a constant factor $a$ on average. In other words, the overlap between two eigenfunctions $|i\rangle$ and $|j\rangle$ of $H_2$ and of a smooth coordinate function decreases exponentially with $n_{ij}$, the total quantum number difference between the wave functions. Second, because of the triangle rule in constraint (iv), couplings among triplets of states are correlated. Strong couplings tend to occur in groups, and weak couplings tend to occur in groups: case (iv) states that if one of two strongly coupled states is strongly coupled to a third state, the other one is also likely to be strongly coupled to the third state; if not, the second one is also likely not to be coupled to the third state.

For sufficiently small $\lambda$, and if all potential constants $v_{ijk\ldots}$ of a given order $n$ were identical, the triangle rule would be exactly obeyed by any Hamiltonian of the form (8). It is a simple consequence of the fact that wave functions with similar nodal structure are strongly coupled by a smooth coordinate function, while wave functions with very different nodal structure are only weakly coupled. In real systems, case (iv) can be only a propensity rule because the magnitudes of individual coupling constants $v_{ijk\ldots}$ can vary substantially, and because higher-order contributions can exceed lower-order contributions as $\lambda$ approaches 1. If matrix elements zero due to symmetry are excluded, case (iv) is obeyed by over 90% of matrix elements in a typical lattice phonon or molecular Hamiltonian with realistic parameter choices [17].

The correlation among matrix elements introduced by cases (ii) and (iv) makes the BSTR model a local random matrix model. It should be noted that these correlations are, if anything, weak compared to real quantum systems modeled by Eq. (8). Additional correlations exist in such systems because the magnitudes of the couplings $v_{ijk}$ vary for a given order $n$. The sources of these variations are twofold. The presence of symmetries constrain matrix elements more strongly than constraint (ii); for example, many matrix elements predicted by constraint (ii) to be nonzero may in fact be zero due to symmetry. The very lack of symmetry can have a similar effect: by replacing the couplings among different modes by a single constant $V$, constraint (ii) implies that a coupling such as $v_{mpr}$ is a geometric mean of the couplings $v_{mmm}$ $v_{ppp}$ and $v_{rrr}$. In real systems $v_{mpr}$ will usually be smaller because the modes are partially localized due to defects or other reasons for the low symmetry of $H$. Therefore, larger variations in the coupling constants $v_{nmp\ldots}$ than suggested by constraint (ii) arise in real systems of low or high symmetry.

TABLE I. Parameters used for the BSTR model calculation in Figs. 4–8, as well as the range sampled in a sequence of $x$ calculations used to sample the statistics of the BSTR model.

| | | |
|---|---|---|
| $V/\hbar\overline{\omega}$ | $8.3\times10^{-4}$ | $2.3\times10^{-4}$–$1.7\times10^{-3}$ |
| $a$ | 0.25 | 0.2–0.3 |
| $N$ | 19 500 | 11 250–57 750 |
| $E/\hbar\overline{\omega}$ | 13 | 1.5–23 |
| $\Delta E/\hbar\overline{\omega}$[a] | $2.6\times10^{-6}$ | $1.2\times10^{-6}$–$4.8\times10^{-6}$ |
| $\mathcal{N}$ | 9 | 6–15 |

[a]Here we treat $\Delta E$ as an independently adjustable model parameter. Strictly speaking, the density of states $\rho=\Delta E^{-1}$ is not independent of $\overline{\omega}$, $\mathcal{N}$, and $E$, but is rather given by $\rho=\sqrt{\mathcal{N}}\Gamma(E/\overline{\omega}+\mathcal{N})/\{\Gamma(E/\overline{\omega})\Gamma(\mathcal{N})\overline{\omega}\}$ [29].

The BSTR model is an excellent laboratory for studying deviations of dephasing line shapes from Lorentzians caused by weak correlations among matrix elements. Is nonexponential dephasing observed, and if so, how is it affected if the constraints in cases (i)–(iv) are relaxed, turning BSTR into a sparse global random matrix?

### B. Numerical results

The dephasing of an initial state evolving under the BSTR Hamiltonian was studied for a variety of models summarized in Table I. Time-independent calculations were carried out by combining the matrix-fluctuation-dissipation (MFD) algorithm with Lanczos iteration to yield spectra [20,21]. Time-dependent propagations of an initial state were performed using the shifted-update-rotation (SUR) symplectic propagator [22]. Matrix elements in the golden rule basis were obtained by applying the LKL inversion to the spectra [15,16]. A single state $|0\rangle$ was assumed to carry the oscillator strength. Convergence was established as a function of $\Delta\omega$ to ensure that long-time dynamics was not affected by truncation of the energy window. In all cases therefore $k\ll\Delta\omega$.

Superimposed on a smooth $P(t)$ decay, a local random matrix ensemble will show fluctuations or ''quantum beats.'' Although these are interesting in their own right [17], here we are mainly concerned with the long-time behavior of the average envelope. In order to highlight the average decay behavior of $P(t)$, a Gaussian smoothing function of full width $t/10$ was applied to all computed decays to remove small high-frequency quantum beats from $P(t)$. The same smoothing was applied to all decays, whether nonexponen-

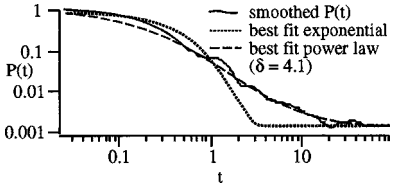


FIG. 4. Survival probability of a typical BSTR matrix with the parameters shown in Table I. The power-law fit of the decay is superior to a weighted exponential fit.

tial (e.g., Fig. 4) or exponential (e.g., Fig. 10). The time window was chosen sufficiently small so as not to affect the average functional form of the faster exponential decays at time $t$ on time scales $>t/10$.

Constraint (ii) indicates that the phases (signs) of the matrix elements were chosen randomly as $\pm 1$. Simulations with several randomly chosen sets of phases, but which kept the magnitudes of matrix elements unchanged, showed that the average decay of an ensemble and the average size of the fluctuations is unaffected by the detailed phase structure. The exact pattern of fluctuations in $P(t)$ varies upon phase randomization, but is excluded from the figures by smoothing as discussed above.

For all calculations $\rho V \gtrsim 1$ was chosen so that $P(t)$ lies just above the delocalization threshold, and decays to the statistical limit $\sigma$ at long times [23,24]. All frequencies and times are expressed in reduced units so $\omega = 2\pi/t$; energy scales are also expressed in units of $2\pi/t$ by using units in which $\hbar = 1$.

A representative $P(t)$ generated using the BSTR model is shown in Fig. 4. That calculation modeled a nine degree of freedom system, with 19 500 basis states distributed in the energy window. Table I summarizes the parameters used for this particular calculation, as well as the range of parameters used in all calculations. The corresponding spectrum computed using the MFD theorem, and the golden rule representation Hamiltonian coupling matrix elements obtained with the LKL inversion are shown in Figs. 5 and 6. $P(t)$ exhibits an early exponential decay phase up to $t=1$, followed by a long-time nonexponential tail. A fit of the smoothed decay confirms power-law behavior over a period roughly 10 times longer than the initial exponential phase. The best-fit power law has an exponent $\delta$ of $4.1 \pm 0.3$, showing that the matrix models a system already significantly above the localization threshold [25]. (The largest possible value of $\delta$ is $\mathcal{N}-1$ in the case of quasimicrocanonical excitation.)

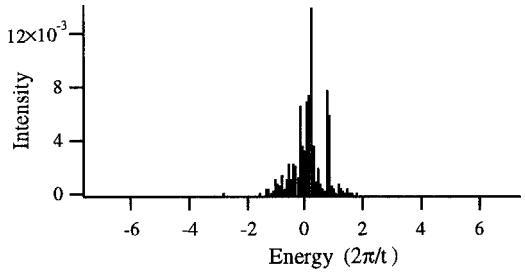


FIG. 5. BSTR line shape corresponding to the dephasing dynamics in Fig. 4.

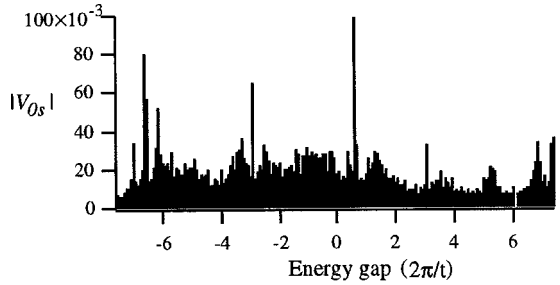


FIG. 6. Absolute value of matrix elements $V_{0s}$ in the ''golden rule'' representation corresponding to Figs. 4 and 5.

Energy-dependent correlations of the coupling strength are clearly visible in the golden rule (GR) Hamiltonian in Fig. 6. Unlike the simple model in Sec. II, fluctuating matrix elements are of course not confined to $\omega \approx 0$. However, regions of smaller and larger matrix elements persist: they bunch together to form dips and peaks when plotted as a function of zero-order state energy. Examination of the BSTR matrices reveals that this structure is due to localization of couplings, which produces ''gateway'' states into which the state $|0\rangle$ must first dephase before coupling to the remainder of the bath. Because the statistical structure of the matrix is independent of the initial state chosen, these gateways have their own gateways, and so on, leading to the hierarchical organization of the time evolution and power-law decay.

Why a slowed decay and not a faster-than-exponential decay? The reason is that gateway states are statistically not likely to occur at exactly $\omega = 0$, but they are likely to occur in the wings of the line shape of state $|0\rangle$. The latter is true because the gateway states *define* the time scale of the early-time dynamics, and hence the overall width $k$ of the line shape, at least in cases where low-order couplings dominate the dynamics. As a result, the coupling distribution of the BSTR ensemble on average fulfills the requirement of Fig. 3 for a generalized Lorentzian line shape: couplings are more likely to enhanced for $0 < \omega < k$ than for $\omega = 0$. The gateway states that correspond to regions of enhanced couplings in the golden rule representation are clearly seen as peaks in the spectrum in Fig. 5 and maxima in the correlated distribution of $V_{0s}$ in Fig. 6.

Figure 7 shows the level spacing distribution, and cumulative level spacing probability of the spectrum in Fig. 5, together with a fit to an integrated Brody distribution

$$W(s,\beta) = 1 - \exp\left\{ -\left[\left[ \Gamma\left(\frac{\beta+2}{\beta+1}\right) s/\langle s\rangle \right]^{(1+\beta)}\right]\right\} \qquad (9)$$

for comparison. $\langle s\rangle$ is the mean level spacing, and $\beta$ a fractional repulsion coefficient that tunes the distribution from Poisson ($\beta = 0$) to Wigner ($\beta = 1$). Level repulsion due to the moderate-to-strong mixing limit and a much closer resemblance to the Wigner function than to a Poisson distributed spacing are clearly seen, with a value for fractional repulsion of $\beta = 0.76$. This is in keeping with the fact that $\delta = 4.1$ lies above the localization threshold, but not at the

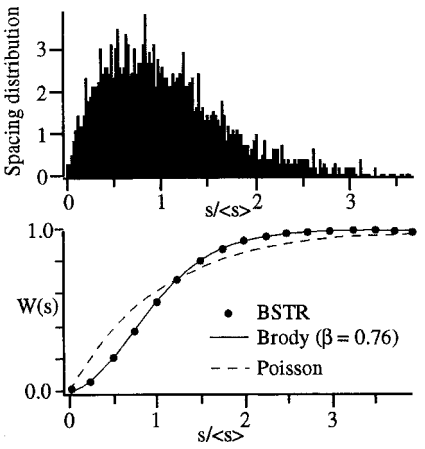


FIG. 7. Level spacing distribution (top) and integrated level spacing distribution $W(s)$ (bottom) for the line shape in Fig. 5, best fitted by a Brody distribution with $\beta=0.76$.

maximal value corresponding to loss of all good quantum numbers. As $V$ in Table I approaches 0, a Poisson distribution is recovered.

As one might expect, the intensity distribution of the spectrum in Fig. 5 nearly follows a Porter-Thomas distribution (Fig. 8). The distribution appears slightly depleted at very large intensities, but these are most sensitive to the proper scaling of the line-shape envelope, which is not a Lorentzian here.

The size distribution of matrix elements $V_{0s}$ in the ''golden rule'' basis is Gaussian for $|V_{0s}|\rangle 0.05|\overline{V_{0s}}|$. (For smaller values the distribution cannot be accurately determined from the present calculations due to rounding errors in the LKL inversion.) The Gaussian distribution is usually assumed when applying the golden rule to the random simulation of spectra, yielding an exponential. The matrix element distribution alone is therefore not sufficient to explain deviations from exponential dynamics.

Not all of the members of the BSTR ensemble have gateways as obvious as the one in Fig. 4. Figure 9 (top) shows the line shape associated with a calculation for $\mathcal{N}=10$. Despite its smoother appearance, this line shape still has large coupling fluctuations. It fits best to $L_{\delta/2}$ with $\delta=8\pm1$, in close accord with the fit (not shown) obtained for its $P(t)$, which yields $\delta=7.1\pm1$.

The question remains of how sensitive the long-time decays are to the correlations present in the ensemble of local

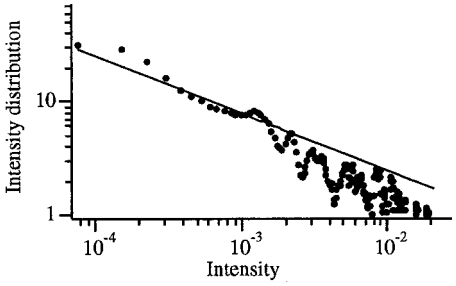


FIG. 8. Intensity distribution for the spectrum in Fig. 5. The solid curve is the Porter-Thomas distribution.

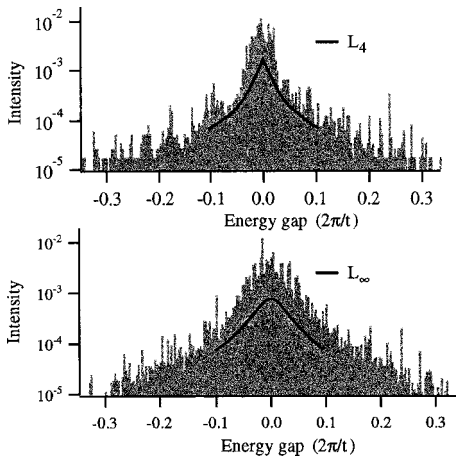


FIG. 9. Top, gray: another BSTR line shape modeling a ten-dimensional quantum system. The solid curve is the best-fit generalized Lorentzian with $\delta=8\pm1$. Bottom: line shape recalculated after shuffling the matrix elements in the ''golden rule'' basis; $\delta=\infty$ fits best.

random matrices. Is a simple sparse matrix sufficient to observe slow long-time dynamics? The correlations in the BSTR model can be destroyed in several increasingly subtle ways.

Consider first the reduction of the BSTR Hamiltonian to the assumption of statistically uncorrelated $V_{i0}$ usually made when the golden rule is applied. This can be achieved by randomly shuffling the $V_{0s}$ shown in Fig. 6, and rediagonalizing the Hamiltonian in the ''golden rule'' representation. Switching the couplings leaves the $\omega_s$ and matrix element size distribution unchanged, so that whatever differences are observed in the corresponding spectrum or $P(t)$ can be attributed only to correlations among the $\omega_s$ and $V_{0s}$. $P(t)$ and $V_{0s}$ as a function of energy for the thus randomized Hamiltonian are shown in Fig. 10. $P(t)$ now fits an exponential decay very well. Nearest-neighbor level spacing statistics are still fitted by a Brody distribution with $\beta=0.74$, indicating that in the ''golden rule'' basis representation of the BSTR Hamiltonian, the level repulsion is already fully encoded in the eigenvalues $\omega_s$, not in the couplings $V_{0s}$. This

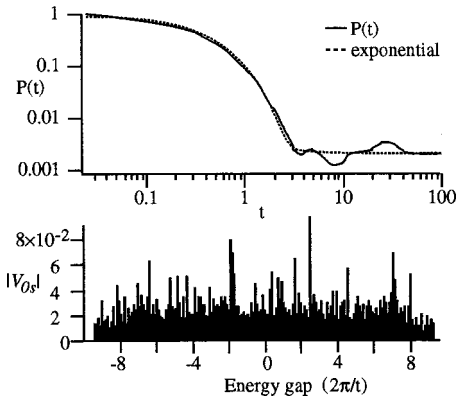


FIG. 10. Survival probability (top) and absolute value of matrix elements $V_{0s}$ (bottom) corresponding to Figs. 4 and 6 after shuffling of the $V_{0s}$ in the ''golden rule'' basis.

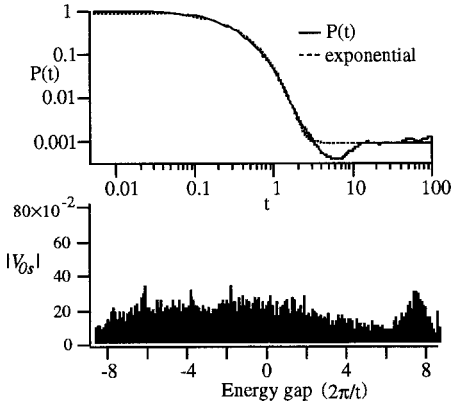


FIG. 11. Survival probability (top) and absolute value of matrix elements $V_{0s}$ (bottom) corresponding to Figs. 4 and 6 after shuffling BSTR matrix elements $h_{ij}$ save those connecting to the initial state $|0\rangle$.

shows that nearest-neighbor level statistics alone are not a good predictor of the nature of the long-time dynamics.

The effect of randomizing the $V_{0s}$ can be equally well illustrated using the spectral line shape instead of the temporal decay. For the $\mathcal{N}=10$ calculation mentioned earlier, Fig. 9 (bottom) shows the line shape obtained when the $V_{0s}$ corresponding to the BSTR line shape in Fig. 9 (top) are shuffled in the golden rule representation. The shuffled line shape is best fitted by a Lorentzian, not the small value of $\delta=8\pm1$ of the original BSTR line shape.

The correlations resulting from the BSTR model can be destroyed more subtly by randomizing the BSTR matrix itself. In the following two examples, the elements $h_{ij}$ of the BSTR matrix in Figs. 5–7 have been shuffled, except for the elements $h_{0i}$ directly coupling the initial state $|0\rangle$. Any changes in the dynamics are therefore not simply due to changing the ''gateway'' states, but rather to the hierarchical structure of states not directly connected to $|0\rangle$. Figure 11 shows $P(t)$ and $V_{0s}$ for the case where the $h_{ij}$ has been shuffled by randomly reassigning $i$ and $j$. The resulting BSTR matrix no longer satisfies the triangle rule. Again, an exponential decay results. No significant correlations remain among the $V_{0s}$ in this case, just as in Fig. 10. The Brody distribution approaches $\beta=0.99$, nearly that of a Gaussian orthogonal ensemble. This is to be expected for a simple sparse global random matrix with sufficiently strong couplings. Matrix sparsity alone cannot encode the correlations that result from a Hamiltonian such as Eq. (9) or its more weakly correlated BSTR model approximations (i) and (iv). A similar result is obtained by simply decreasing the variance of the matrix elements $h_{ij}$ by letting $a\rightarrow1$.

The triangle rule in case (iv) can be broken in an even more subtle fashion. Figure 12 shows $P(t)$ and the $V_{0s}$ when only the *values* of the $h_{ij}$ above a certain threshold have been randomized, but not the locations *i,j* themselves. This leaves the connectivity of the BSTR matrix unchanged, but destroys the triangle rule for the largest matrix elements. $P(t)$ is again nearly exponential, and only weak correlations on a larger energy scale than in Fig. 6 persist among the $V_{0s}$. In this case, the Brody distribution ($\beta=0.85$) is intermediate between the original and randomly shuffled BSTR matrix.

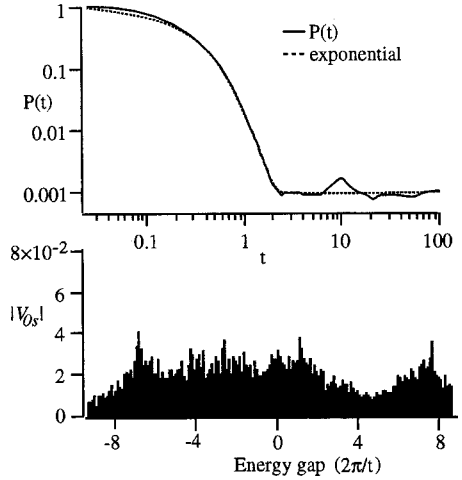


FIG. 12. Survival probability (top) and absolute value of matrix elements $V_{0s}$ (bottom) corresponding to Figs. 4 and 6 after shuffling BSTR matrix elements $h_{ij}>Va^2$, save those connecting to the initial state $|0\rangle$.

## IV. DISCUSSION AND EXPERIMENTAL EXAMPLES

A simple intuitive picture can be given for the results obtained in Sec. III. Quantum diffusion in an $\mathcal{N}$-dimensional state space could in principle always be a power-law process. However, the simulations show that the evolving wave packet probes the effective diffusion dimension $\delta$ only when the Hamiltonian can be brought into a locally coupled form. Otherwise, the dynamics remain exponential even for a sparse matrix, corresponding to an effectively infinite-dimensional diffusion manifold.

The finite $\delta$ arises because the HLRM structure of the BSTR Hamiltonian mimics the preservation of a local set of approximately conserved quantum numbers. Conditions (ii) and (iv) define a rudimentary state space by introducing a distance measure $n_{ij}$. Of course, a single distance measure cannot map out all the coupling anisotropies that may be present in the full state space of an $\mathcal{N}$-dimensional quantum system. Nonetheless, conditions (ii) and (iv) prevent direct flow to far away parts of the quantum state space, and dephasing of the wave packet is retarded. Above the full localization threshold at $\rho V=1$, the state space of the BSTR model remains connected, so an evolving wave packet can eventually sample it. The structure of the BSTR Hamiltonian cannot prevent statistical coverage of the state space by a wave packet at infinite time.

The BSTR model does not encode any of the details of the locally conserved quantum numbers. Thus, power-law dephasing is expected in actual physical systems even in cases when the approximately conserved quantum numbers are strongly dependent on the location in state space. In such a case the evolving wave packet is embedded in a manifold of dimension less than $\mathcal{N}$ but which nonetheless connects arbitrary regions of phase space. (In action space, such a manifold would be labeled fractal of dimension $\delta$, and perhaps such a label is useful even for a discrete quantum state space.)

In the BSTR model, the multiple time scales of the

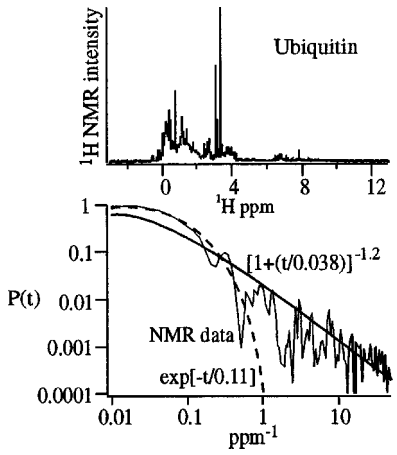


FIG. 13. NMR spectrum (top) and corresponding $P(t)$ (bottom) of the protein human ubiquitin. The spectrum was acquired in $D_2O$ solution at 1 mM protein concentration on a 500-MHz NMR.

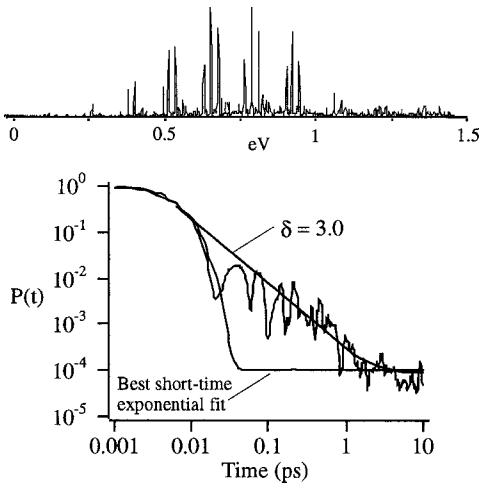


FIG. 14. Experimental spectrum of the molecule $SCCl_2$ with six vibrational modes (top), and quantum dynamics for a randomly chosen initial vibrational state $|233222\rangle$ computed from the experimentally derived Hamiltonian (bottom).

power-law decay cannot be attributed to a specific set of quantum numbers or resonances that initiate population transport in state space. In real physical systems such as the ones discussed below, one could inquire which conserved quantum numbers or local sets of conserved quantum numbers are specifically responsible for the various stages of $P(t)$. The answer to this question will provide much deeper knowledge about the mechanism of dephasing and quantum transport in real systems, and remains to be studied in detail.

The requirements embodied in Eq. (8) are quite general. This raises the question as to whether power-law decays can be deduced from experimentally observed spectra. One such set of spectra is furnished by coupled nuclear spins $s_i=1/2$, interacting in the isotropically averaged limit via the Hamiltonian

$$H=B_z\sum_i (1-\sigma_i)s_{iz}+\sum_{i,j}^{n\prime} J_{ij}s_{iz}s_{jz}, \qquad (10)$$

where the $\prime$ in the summation indicates that only nearest neighbors can interact. $\sigma_1$ is a result of variations in the local spin environment. Although Eq. (10) corresponds to coupled two-level systems, not to a set of coupled oscillators such as Eq. (8), similarities abound: the two-level nature introduces strong anharmonicity, and nearest-neighbor interactions introduce a local structure to the Hamiltonian. Equation (11) can be approximately realized by the proton NMR spectrum of a large molecule tumbling freely in a solvent. Figure 13 shows a proton nuclear magnetic resonance spectrum of the protein ubiquitin, which contains over 150 protons. In such a molecule, only spins in direct contact, or connected by a bridge of exactly two heavier atoms, can interact significantly. The $P(t)$ derived from the spectrum via

$$P(t)=\int d\omega \int d\omega' I(\omega)I(\omega')\cos([\omega-\omega']t) \qquad (11)$$

in Fig. 13 has a power-law tail, indicative of the locally coupled nature of $H$ in Eq. (11). (The tail has nothing to do with the dephasing induced by the solvent, which causes a purely exponential response resulting from linewidths $<0.01$ ppm on the scale of Fig. 13; the number of solvent degrees of freedom interacting with ubiquitin is too large for the corresponding generalized Lorentzian to be distinguished from a Lorentzian line shape.)

Another example is shown in Fig. 14: we have recently studied the sequence of eigenstates corresponding to the quantized vibrational motions of the $\mathcal{N}=6$ molecule $SCCl_2$ [5,26]. The hierarchical structure of the experimental spectrum in Fig. 14 is evident, and indicative of a localized coupling structure of $H$ up to energies where the molecule dissociates. In fact, the experimentally determined Hamiltonian

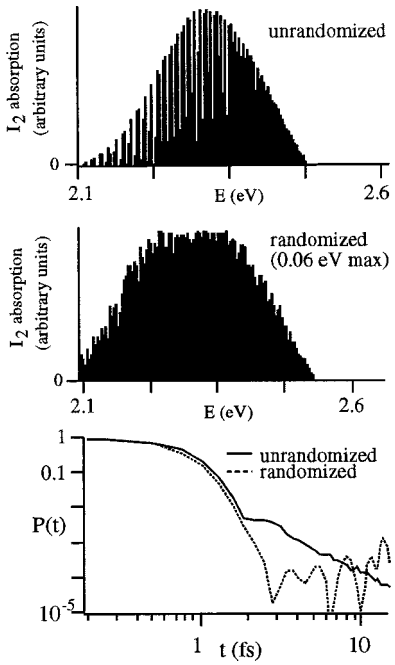


FIG. 15. Vibrational absorption spectrum of the $\tilde{B}$ electronic state of $I_2$ (top); the shuffled version of the spectrum (middle), and the corresponding survival probabilities (bottom).

for this system has exactly the structure of Eq. (8) [26] and satisfies the constraints in cases (i)–(iv) with good accuracy [17]. Figure 14 also shows the $P(t)$ derived from a quantum dynamics calculation with a randomly chosen initial state, using a Hamiltonian fitted to the experimental spectrum [5]. The dephasing decay is well approximated by a power law with $\delta \approx 3$ at longer times (but levels off at the statistical limit). Even at energies of more than 1 eV (the characteristic energy scale in Eq. (8) is $\omega_i = 0.037 - 0.14\,\mathrm{eV}$), $\delta$ is smaller than the maximum possible value 5, indicating two locally conserved good quantum numbers. (The fact that the spectrum does decay to the statistical value at long times indicates that they are only locally conserved.)

It should be noted that slow long-time decays can arise even from a completely regular system if there are strong correlations among the parameters of the Hamiltonian. Consider the rovibrational spectrum of the diatomic molecule $I_2$ in the $\tilde{B}$ electronic state [27,28]. Figure 15 illustrates the spectrum and corresponding $P(t)$. In the second spectrum the line positions have been randomized by $\pm 0.06$ eV. The corresponding $P(t)$ progresses from a power law to a simple exponential with increasing randomization. A randomization of $\pm 0.03$ eV is required to recover an exponential decay; this is on the scale $\omega \approx 0.03\,\mathrm{eV}$ of the vibrational frequency of the I—I bond. The highly regular structure of energy levels that is given by an expansion of the type

$$E(J,\nu) = \sum_{n,m} Y_{nm}[J(J+1)]^n (\nu + \tfrac{1}{2})^m \qquad (12)$$

is responsible for the slow decay here. ($J$ is the rotational and $\nu$ the vibrational quantum number, and the $Y_{nm}$ decrease rapidly with $n$ and $m$.) Such correlations do not usually exist among the frequencies $\omega_m$ of the zero-order Hamiltonian $H_2$ in Eq. (8), but when they exist, must be taken into account in assessing power-law decays.

In conclusion, a local random matrix that satisfies an exponential scaling law, *and* a localization criterion such as the triangle rule for its off-diagonal matrix elements, produces a slower-than-exponential dephasing of quantum wave packets before the statistical limit is reached. Elimination of either the scaling property or the triangle rule reverts the dynamics to simply exponential. The structure of the matrix apparently mimics the conservation of local good quantum numbers. Various types of spectroscopies of molecular systems reveal power-law behavior consistent with the HLRM model. Indeed, molecular spectroscopy provides an ideal tool for the study of mesoscopic systems and their dephasing or decoherence properties because large numbers of transitions can usually be observed in such spectra.

## ACKNOWLEDGMENTS

This work was supported by the David and Lucile Packard Foundation and by the National Science Foundation. The authors would like to thank J. Ervin for acquiring the ubiquitin spectrum.

[1] T. Mercouris and C. A. Nicolaides, J. Phys. B **29**, 1151 (1995).
[2] D. Boyanovsky, C. Destri, H. J. d. Vega, R. Holman, and J. Salgado, Phys. Rev. D **57**, 7388 (1998).
[3] S. Sinha, Phys. Lett. A **228**, 1 (1997).
[4] C. H. Mak and D. Chandler, Phys. Rev. A **44**, 2352 (1991).
[5] V. Wong and M. Gruebele, J. Phys. Chem. **103**, 10083 (1999).
[6] S. A. Schofield and P. G. Wolynes, J. Chem. Phys. **98**, 1123 (1993).
[7] G. Casati, G. Maspero, and D. L. Shepelyansky, Phys. Rev. Lett. **82**, 524 (1999).
[8] M. Gruebele and R. Bigwood, Int. Rev. Phys. Chem. **17**, 91 (1998).
[9] M. Gruebele, Adv. Chem. Phys. **114**, 193 (2000).
[10] M. A. Sepulvéda and E. J. Heller, J. Chem. Phys. **101**, 8016 (1994).
[11] J. Svitak, Z. Li, J. Rose, and M. E. Kellman, J. Chem. Phys. **102**, 4340 (1995).
[12] M. J. Davis, J. Chem. Phys. **98**, 2614 (1993).
[13] M. L. Mehta, *Random Matrices* (Academic Press, San Diego, 1991).
[14] M. Gruebele, Proc. Natl. Acad. Sci. U.S.A. **95**, 5965 (1998).
[15] W. D. Lawrance and A. E. W. Knight, J. Phys. Chem. **89**, 917 (1985).
[16] K. K. Lehmann, J. Phys. Chem. **95**, 7556 (1991).
[17] M. Gruebele, J. Phys. Chem. **100**, 12 183 (1996).
[18] E. J. Heller, J. Phys. Chem. **86**, 1822 (1982).
[19] M. V. Berry and M. Tabor, Proc. R. Soc. London, Ser. A **356**, 375 (1977).
[20] M. Gruebele, J. Phys. Chem. **100**, 12178 (1996).
[21] M. Gruebele, J. Chem. Phys. **104**, 2453 (1996).
[22] R. Bigwood and M. Gruebele, Chem. Phys. Lett. **233**, 383 (1995).
[23] P. Pechukas, Chem. Phys. Lett. **86**, 553 (1982).
[24] D. E. Logan and P. G. Wolynes, J. Chem. Phys. **93**, 4994 (1990).
[25] S. A. Schofield and P. G. Wolynes, J. Phys. Chem. **99**, 2753 (1995).
[26] R. Bigwood, B. Milam, and M. Gruebele, Chem. Phys. Lett. **287**, 333 (1998).
[27] S. Gerstenkorn and P. Luc, J. Phys. (France) Lett. **46**, 867 (1985).
[28] S. Gerstenkorn and P. Luc, *Atlas du Spectre d' Absorption de la Molecule d'Iode, 14,800–20,000 cm-1; Complement: Identification des Transitions du Systeme (B-X)* (Editions du CNRS: Diffusion, Presses du CNRS, Paris, 1986).
[29] R. Pearman and M. Gruebele, J. Chem. Phys. **108**, 6561 (1998).